

Continuous-Time Neural Networks Can Stably Memorize Random Spike Trains

Hugo Aguetaz and Hans-Andrea Loeliger

{aguetaz, loeliger}@isi.ee.ethz.ch

ETH Zürich, Dept. of Information Technology & Electrical Engineering

Keywords: Spiking neural networks, stable memorization.

Abstract

The paper explores the capability of continuous-time recurrent neural networks to store and recall precisely timed spike patterns. We show (by numerical experiments) that this is indeed possible: within some range of parameters, any random score of spike trains (for all neurons in the network) can be robustly memorized and autonomously reproduced with stable accurate relative timing of all spikes, with probability close to one. We also demonstrate associative recall under noisy conditions.

In these experiments, the required synaptic weights are computed offline, to satisfy a template that encourages temporal stability.

1 Introduction

Biological neural networks work in continuous time, without a clock, and with (apparently) imprecise and noisy neurons (Kandel et al., 2021). It is thus not obvious how memories can be stably represented at all. Nonetheless, biological neural networks appear to have impressive storage capacity and the ability to control muscles with high temporal precision. Understanding this better is of interest in its own right, and it may give ideas for designing future neuromorphic hardware (Indiveri & Liu, 2015; Grimaldi et al., 2023; Rubino et al., 2023; Dalgaty et al., 2024).

It is an old idea that memories can be encoded as stable attractors of the network dynamics (Amit, 1989; Poucet & Save, 2005; Ramsauer et al., 2021). The classical Hopfield networks (Hopfield, 1982) works with point attractors, and cyclic attractors have been proposed for representing repetitive biological behaviors such as breathing, running, or flying (Eliasmith, 2005). A related concept from the literature are polychronous groups of neurons as observed by Izhikevich (2006).

We also note that many studies of neural dynamics (of continuous-time recurrent networks) have focused on networks in which the weights are randomly assigned (i.e., not learned or precomputed), and this setting has been observed to promote chaotic behavior (Banerjee et al., 2008).

In this paper, we consider an extreme version of memorization, viz., the stable memorization of arbitrary spike trains as in Fig. 1, with exact relative timing of all spikes of all neurons in the network. Our main result is the empirical observation that, with suitable qualifications, this is indeed possible: in some range of parameters, for any random

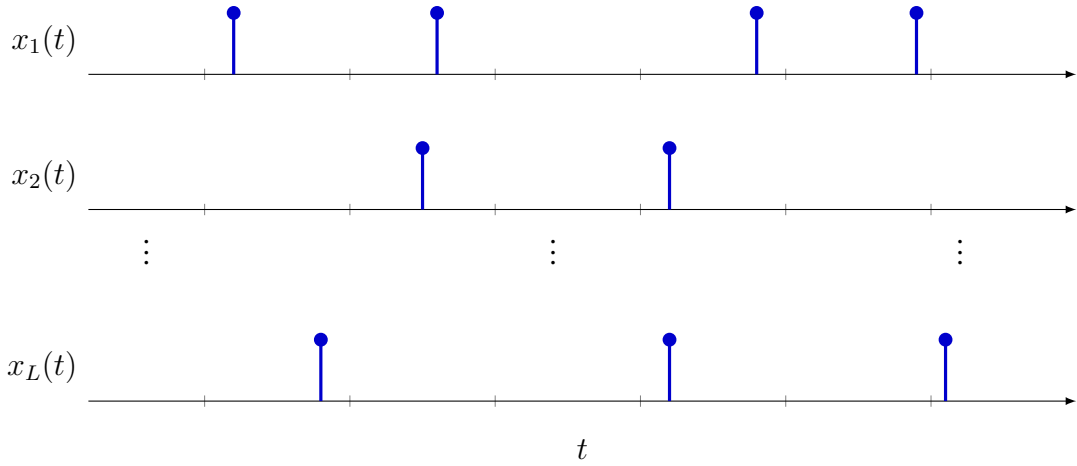


Figure 1: A score of spike trains x_1, \dots, x_L produced by L neurons, with minimum separation τ_0 (= distance between the tickmarks) between spikes.

score of spike trains, there exist synaptic weights (with probability close to one) such that the network can autonomously reproduce all these spikes (with accurate relative timing), even in the presence of substantial disturbances. To the best of our knowledge, this has not been demonstrated (and not even suggested) before.

Whether such spike-level temporal precision is used in biological neural networks remains to be seen. In any case, the mathematical possibility (which we demonstrate in this paper) does seem to open interesting perspectives for neuromorphic engineering.

For technical convenience, we will formulate the memorization problem in terms of cyclic attractors, but this formulation is not essential.

We will work with (a variation of) a standard continuous-time neural network model with random transmission delays. The latter are essential; we thus reconfirm the observation from Izhikevich (2006) that axonal delays are not a nuisance, but a valuable resource.

We will use a new algorithm to compute the synaptic weights in a way that encourages temporal stability. While we do not claim biological plausibility for this algorithm, it is at least neuron local, i.e., the synaptic weights to each neuron are computed using only (spike time) information that this neuron sees in its own operation.

The paper is structured as follows. The network model is defined in Section 2. The precise problem statement and the main experimental results are given in Section 3. The computation of the synaptic weights and further experimental results are described in Section 4. The capacity of such networks is discussed in Section 5. In Section 6, the results of Section 3 are complemented with an eigenvalue analysis of a linearized version of the network model. Associative recall is demonstrated in Section 7, and the conclusions are offered in Section 7.2. Some technical details are given in the Appendices. The software for the experiments in this paper is available on GitHub¹.

¹<https://github.com/haguettaz/RSNN>

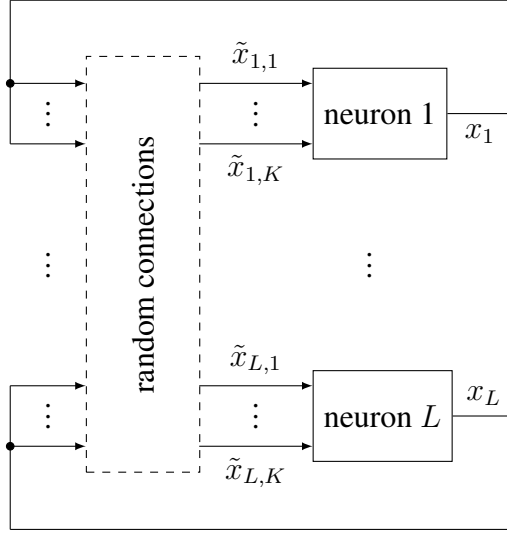


Figure 2: Network structure with L neurons (producing spike trains x_1, \dots, x_L) connected at random. Every neuron receives the same number K of inputs.

2 Spiking Neural Network Model

2.1 Spike Trains and Network Structure

We will use recurrent networks with the structure of Fig. 2. There are L neurons, producing spike trains $x_1(t), \dots, x_L(t)$ as illustrated in Fig. 1. Every neuron has K inputs, and each of these inputs is randomly selected (independently and with uniform probability) from $x_1(t), \dots, x_L(t)$. The inputs of neuron ℓ are denoted $\tilde{x}_{\ell,1}, \dots, \tilde{x}_{\ell,K}$. Note that both parallel connections (between the same pair of neurons) and self-connections (some neuron feeding itself) are allowed. Note also that K and L are unrelated: both $K \ll L$ and $K \gg L$ are possible.

Each connection has its own axonal delay, which, however, will be viewed as part of the neuron model, which will be specified below.

For mathematical convenience, the spikes are represented by Dirac deltas. Thus each spike train $x_\ell(t)$ is of the form

$$x_\ell(t) = \sum_{s \in \mathcal{S}_\ell} \delta(t - s), \quad (1)$$

where $\mathcal{S}_\ell \subset \mathbb{R}$ is the (discrete) set of firing times of neuron ℓ . The neuron model (specified below) guarantees that any two spikes of the same neuron are separated by at least $\tau_0 > 0$, which is the natural unit of time in the network.

2.2 The Spiking-Neuron Model

We will use a version of the Spike Response Model (SRM) (Gerstner, 1995; Kistler et al., 1997), which offers just enough biological (or physical) realism to be useful for our purpose.

The pivotal quantity of each neuron is its potential $z_\ell(t)$: the neuron fires (i.e., it produces a spike) whenever $z_\ell(t)$ crosses a threshold $\theta_\ell(t)$, as will be detailed in Sec. 2.3.

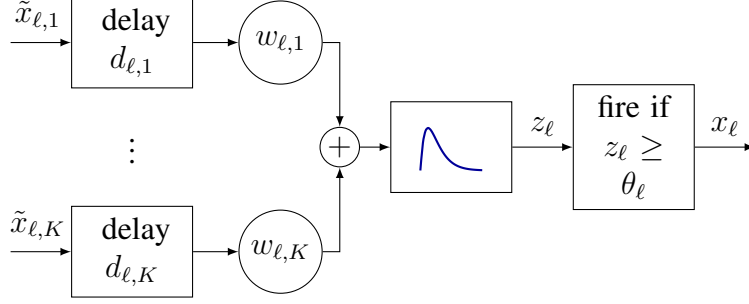


Figure 3: Neuron model with potential (2).

As illustrated in Fig. 3, $z_\ell(t)$ develops according to

$$z_\ell(t) = \sum_{k=1}^K w_{\ell,k} \sum_{s \in \tilde{\mathcal{S}}_{\ell,k}} h(t - d_{\ell,k} - s) \quad (2)$$

where $\tilde{\mathcal{S}}_{\ell,k}$ is the (discrete) set of firing times of $\tilde{x}_{\ell,k}$ and

$$h(t) \triangleq \begin{cases} \frac{t}{\beta} \exp\left(1 - \frac{t}{\beta}\right) & \text{if } t \geq 0 \\ 0 & \text{if } t < 0. \end{cases} \quad (3)$$

It is easily seen that the pulse (3) peaks at $t = \beta$ with $\max_t h(t) = 1$. Therefore, the contribution of any single spike in $\tilde{x}_{\ell,k}$ to (2) is bounded in magnitude by $|w_{\ell,k}|$.

The exact pulse shape (3) is not essential: any similar pulse shape would do.

The individual axonal delays $d_{\ell,k}$ are chosen at random (independently and uniformly between d_{\min} and d_{\max}), but fixed during operation. These delays are essential for this paper.

The weights $w_{\ell,k} \in \mathbb{R}$ are available for learning. We will always use bounded weights.

2.3 Refractory Period and Threshold Noise

A neuron fires when its potential (2) exceeds a threshold θ_ℓ , after which the neuron cannot fire for a period of duration τ_0 .

All neurons have the same fixed nominal threshold $\theta_0 > 0$. However, neuronal computation is subject to noise at various levels (Faisal et al., 2008), which manifests in shifted, false, or missed firings. In this paper, the primary way to model such noise is to work with a random threshold $\theta_\ell(t)$ as follows: after each firing of neuron ℓ , its threshold θ_ℓ (for the next firing) is newly (and independently) sampled from a Gaussian distribution with mean θ_0 and variance σ_θ^2 , as illustrated in Fig. 4.

Note that this noise model can capture many different effects: small deviations from θ_0 result primarily in shifted firings while large deviations from θ_0 can suppress or produce firings.

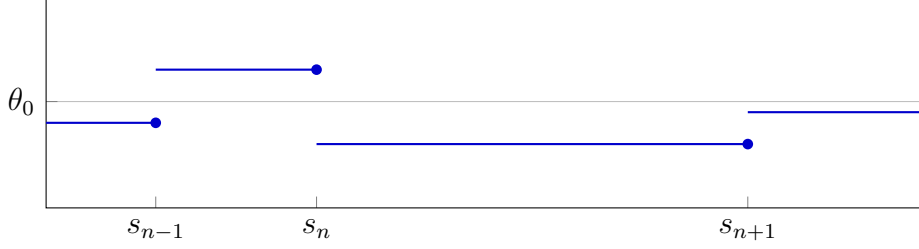


Figure 4: Noisy threshold $\theta_\ell(t)$ with firings at times s_{n-1} , s_n , s_{n+1} .

3 Problem Statement and Main Result

Suppose we are given

- (a) a network as described in Sec. 2, and
- (b) a prescribed score of spike trains $\check{x} = (\check{x}_1, \check{x}_2, \dots, \check{x}_L)$ as in Fig. 1.

Do there exist weights $w_{\ell,k}$ (for all neurons) such that the network (when properly initialized) can autonomously (i.e., without an external input) and stably reproduce the prescribed firing score?

The main result of this paper is that the answer is yes (in some range of parameters, with some qualifications), and we can actually compute such weights. However, the problem statement requires a number of clarifications.

3.1 Just Standard Supervised Learning?

Obviously, the stated problem may be viewed as a form of supervised learning, where each neuron is trained to predict its next prescribed firing. However, standard methods of supervised learning (Wang et al., 2020) will not enable the network to stably reproduce the prescribed score of spike trains autonomously: small errors in the firing times will quickly accumulate and the temporal coherence of the spike score will be lost (cf. the first row of Table 3 and Table 5).

Therefore, in this paper, it is critical to compute the synaptic weights in a way that encourages temporal stability.

3.2 The Prescribed Score of Spikes: Periodic and Random

In order to simplify the discussion, the prescribed score of spike trains is periodic with period $T \gg \tau_0$. In other words, we wish the memorized spike score to be a cyclic attractor. (The generalization to multiple cyclic attractors is obvious and will be demonstrated in Sec. 7.)

We will consider *random* periodic spike scores, which we wish the network to reproduce with probability close to one. In fact, it is easy to see that there exist spike scores that the network cannot be made to reproduce², but we wish the probability of all such unfeasible spike scores to be close to zero.

²E.g., a neuron cannot fire if it receives no firings at any of its synapses. Or a neuron sees the same past inputs twice, but is supposed to fire only in one of the two cases.

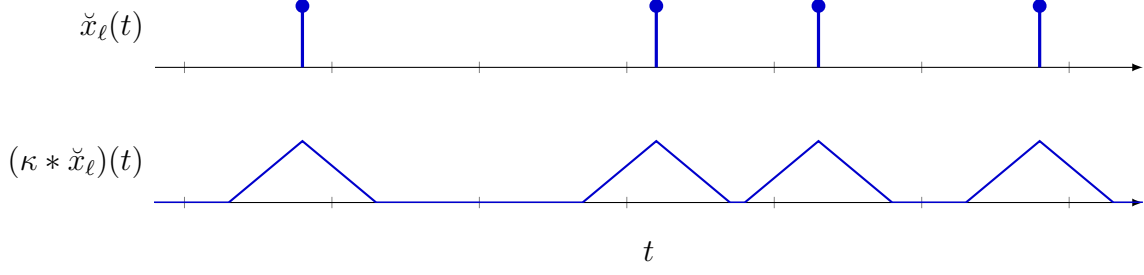


Figure 5: The (T -periodic) function $(\kappa * \check{x}_\ell)(t)$ in (4), (5), and (7). The distance between the tickmarks is τ_0 .

The L random spike trains (one for each neuron) are generated independently. The probability law of each spike train is a suitably modified Poisson process with spikes separated by at least τ_0 . Both the exact definition and the practical generation (i.e., the sampling) of such random spike trains are detailed in Appendix 7.2. In particular, the expected number of spikes (of each neuron, per period T) as a function of the firing rate λ is given by (B.13) and plotted in Fig. 11.

3.3 Measuring Accuracy and Stability

In our numerical experiments, the accuracy of reproduction over some period $[t_0, t_0 + T)$ will be measured by the precision

$$\text{pr}(t_0) \triangleq \frac{1}{L} \sum_{\ell=1}^L \frac{1}{|\mathcal{S}_\ell^{t_0}|} \sum_{s \in \mathcal{S}_\ell^{t_0}} (\kappa * \check{x}_\ell)(s - \hat{\tau}) \quad (4)$$

and the recall

$$\text{rc}(t_0) \triangleq \frac{1}{L} \sum_{\ell=1}^L \frac{1}{|\check{\mathcal{S}}_\ell^0|} \sum_{s \in \mathcal{S}_\ell^{t_0}} (\kappa * \check{x}_\ell)(s - \hat{\tau}), \quad (5)$$

where

- $\check{x}_\ell(t)$ is the (periodic) spike train prescribed for neuron ℓ ,
-

$$\kappa(t) \triangleq \begin{cases} 1 - 2|t|/\tau_0, & |t| \leq \tau_0/2 \\ 0, & \text{otherwise} \end{cases} \quad (6)$$

is a triangular kernel that covers at most one spike (cf. Fig. 5),

- $\check{\mathcal{S}}_\ell^0$ is the set of firing times of \check{x}_ℓ within $[0, T)$,
- $\mathcal{S}_\ell^{t_0}$ is the set of actual firing times of neuron ℓ within $[t_0, t_0 + T + c) \approx [t_0, t_0 + T)$, where c adjusts for border effects³ that can arise since the actual firings are not

³Specifically, c is the largest element of $\{-\tau_0, 0, \tau_0\}$ such that $\min_k |s + kT - s'| > \tau_0$ for all $s \neq s' \in \mathcal{S}_\ell^{t_0}$, see Fig. 6.

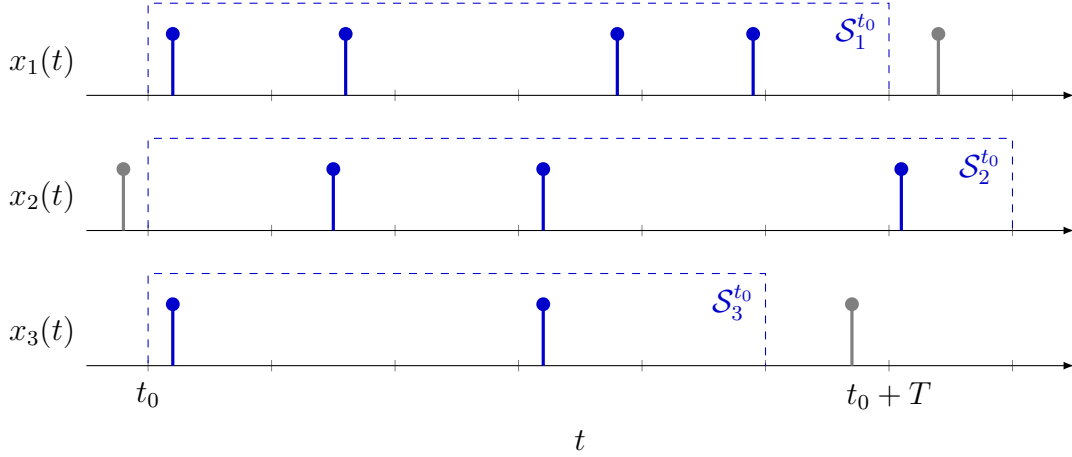


Figure 6: The window $[t_0, t_0 + T + c) \approx [t_0, t_0 + T)$ in the definition of $\mathcal{S}_\ell^{t_0}$ in (4), (5), and (7). The distance between the tickmarks is τ_0 .

strictly periodic,

- and

$$\hat{\tau} \triangleq \operatorname{argmax}_{0 \leq \tau < T} \sum_{\ell} \sum_{s \in \mathcal{S}_\ell^{t_0}} (\kappa * \check{x}_\ell)(s - \tau) \quad (7)$$

is the best temporal adjustment between $\mathcal{S}_\ell^{t_0}$ and $\check{\mathcal{S}}_\ell^0$.

Note that $0 \leq \operatorname{pr}(t_0) \leq 1$, and $\operatorname{pr}(t_0) = 1$ if and only if every spike in $\mathcal{S}_\ell^{t_0}$ is perfectly matched by a spike in $\check{\mathcal{S}}_\ell^0$. Likewise, $0 \leq \operatorname{rc}(t_0) \leq 1$, and $\operatorname{rc}(t_0) = 1$ if and only if every spike in $\check{\mathcal{S}}_\ell^0$ is perfectly matched by a spike in $\mathcal{S}_\ell^{t_0}$.

Clearly, (4) and (5) coincide if $|\mathcal{S}_\ell^{t_0}| = |\check{\mathcal{S}}_\ell^0|$; in this case, low values of $\operatorname{pr}(t_0)$ and $\operatorname{rc}(t_0)$ indicate strong firing jitter. The condition $\operatorname{pr}(t_0) \gg \operatorname{rc}(t_0)$ indicates many missing firings while $\operatorname{pr}(t_0) \ll \operatorname{rc}(t_0)$ indicates many false firings, cf. Sec.3.5 and Sec.7.

Finally, we note that $\check{\mathcal{S}}_\ell^0$ is (practically) never empty, so (5) is always well defined. By contrast, $\mathcal{S}_\ell^{t_0}$ can be empty (i.e., the network has stalled), in which case we *define* the precision (4) to be zero.

3.4 Drift and Very-Long-Term Stability

Any two physical clocks that are not synchronized will inevitably drift away from each other (unless there is absolutely no noise). This applies also to the problem statement in this section: the threshold noise may have a net effect of pushing all spikes forward (or backward) in time, which is unrecoverable (see also Sec. 6). Therefore, our measures of precision (4) and recall (5) cover only a single period rather than the whole time axis.

Moreover, the reader may have noticed that, with threshold noise as in Sec. 2.3, the experimentally observed temporal stability (cf. Sec. 3.5) cannot last forever. For example, it is possible that the momentary thresholds $\theta_\ell(t)$ (i.e., θ_0 plus threshold noise) of all neurons are set to such high values that all firings are suppressed, which stalls the

Table 1: Accuracy of autonomous reproduction with threshold noise. Every row summarizes 100 repetitions of the same experiment.

L	σ_θ/θ_0	pr($20T$)			rc($20T$)		
		min	med	max	min	med	max
50	0.05	0.972	0.977	0.979	0.972	0.977	0.979
	0.1	0.945	0.954	0.959	0.945	0.954	0.959
	0.15	0.000	0.926	0.937	0.000	0.926	0.937
100	0.05	0.974	0.977	0.978	0.974	0.977	0.978
	0.1	0.949	0.954	0.958	0.949	0.954	0.958
	0.15	0.000	0.926	0.935	0.000	0.926	0.935
200	0.05	0.975	0.977	0.978	0.975	0.977	0.978
	0.1	0.949	0.953	0.956	0.949	0.953	0.956
	0.15	0.083	0.926	0.935	0.069	0.926	0.935
500	0.05	0.975	0.977	0.978	0.975	0.977	0.978
	0.1	0.952	0.954	0.956	0.952	0.954	0.955
	0.15	0.894	0.926	0.932	0.892	0.926	0.932

network in that state. However, in some range of parameters, the probability of such derailments is so small that they are never observed in numerical experiments.

3.5 Experimental Results

Some exemplary experimental results are reported in Table 1, which shows the precision (4) and the recall (5) for different values of L (the number of neurons) and σ_θ (the standard deviation of the threshold noise). The values of all other parameters are listed in Table 2, which shows the default values of all parameters in all numerical experiments of this paper. With λ and T as in Table 2, the expected total number of spikes (of all neurons, during one period of duration T) is about $7L$ (cf. Fig. 11 in Appendix 7.2).

In these experiments, the synaptic weights are computed as described in Sec. 4 (below). The network is initialized with the exact correct firing times; then it is left to operate autonomously (with threshold noise as in Section 2.3). After about five periods, the precision and the recall have reached a steady state, which is reported in Table 1 (after 20 periods); running the simulations longer does not change anything (but see Sec. 3.4 for extreme time scales).

Every row of Table 1 summarizes 100 repetitions of the same experiment, each with a new random network and a new random prescribed firing score; every row reports the median, the minimum, and the maximum values of (4) and (5) of all 100 repetitions.

These experiments are representative of large numbers of similar experiments, with qualitatively similar results.

Table 2: Default values of the model parameters in all numerical experiments.

Symbol	Description	Default Value
L	number of neurons (Sec. 2.1)	200
K	number of inputs per neuron (Sec. 2.1)	500
β	input kernel parameter (Sec. 2.2)	τ_0
d_{\min}	minimal axonal delay (Sec. 2.2)	$0.1 \tau_0$
d_{\max}	maximal axonal delay (Sec. 2.2)	$10 \tau_0$
θ_0	nominal threshold (Sec. 2.3)	1
σ_θ	standard deviation of threshold noise (Sec. 2.3)	$0.1 \theta_0$
T	period of firing score (Sec. 3.2 and App. 7.2)	$50 \tau_0$
λ	random-firing rate (App. 7.2)	$0.2/\tau_0$
ε_s	width of firing zone (10), (11)	$0.2 \tau_0$
θ_r	maximum potential (10)	0
$\dot{\theta}_s$	minimal potential slope (11)	$2 \theta_0/\tau_0$
w_b	weight bound (12)	$0.2 \theta_0$
ν	weight penalty (13)	2

4 Computing the Synaptic Weights

The synaptic weights $w_{\ell,1}, \dots, w_{\ell,K}$ are computed to satisfy the constraints

$$z_\ell(t) \geq \theta_0 \quad \text{if } t \in \check{S}_\ell \quad (8)$$

$$z_\ell(t) < \theta_0 \quad \text{if } s - \varepsilon_s < t < s \text{ for some } s \in \check{S}_\ell \quad (9)$$

$$z_\ell(t) < \theta_r \quad \text{unless } s - \varepsilon_s < t < s + \tau_0 \text{ for some } s \in \check{S}_\ell \quad (10)$$

$$\dot{z}_\ell(t) > \dot{\theta}_s \quad \text{if } s - \varepsilon_s < t < s + \varepsilon_s \text{ for some } s \in \check{S}_\ell \quad (11)$$

$$|w_{\ell,k}| \leq w_b \quad (12)$$

where $x_\ell(t) = \check{x}_\ell(t)$ is the prescribed periodic spike train for neuron ℓ , \check{S}_ℓ is the set of firing times of \check{x}_ℓ , and $\dot{z}_\ell(t)$ is the derivative of $z_\ell(t)$ with respect to t .

Conditions (8)–(11) are illustrated in Fig. 7. (The meaningful range of the parameters in (10)–(12) is limited by $0 < w_b < \theta_0$, $\dot{\theta}_s \geq 0$, $\theta_r < \theta_0$.)

Since all firings are prescribed, both $z_\ell(t)$ and $\dot{z}_\ell(t)$ are linear functions of $w_{\ell,1}, \dots, w_{\ell,K}$. Therefore, (8)–(12) is a feasibility problem with linear constraints, with no coupling between the neurons.

Similar conditions for the potential $z_\ell(t)$ have been used in (Lee et al., 2017), which, however, did not address temporal stability. The minimal-slope condition (11) appears to be a new ingredient, which is essential for temporal stability; the effect of this condition is demonstrated in Table 3 (see also Table 5).

The temporal stability is further enhanced by choosing the weights to minimize

$$\sum_{k=1}^K |w_{\ell,k}|^\nu \quad (13)$$

with $\nu = 1$ (resulting in sparse weights) or $\nu = 2$, subject to (8)–(12). The effect of this additional regularization is demonstrated in Table 4 (see also Table 6).

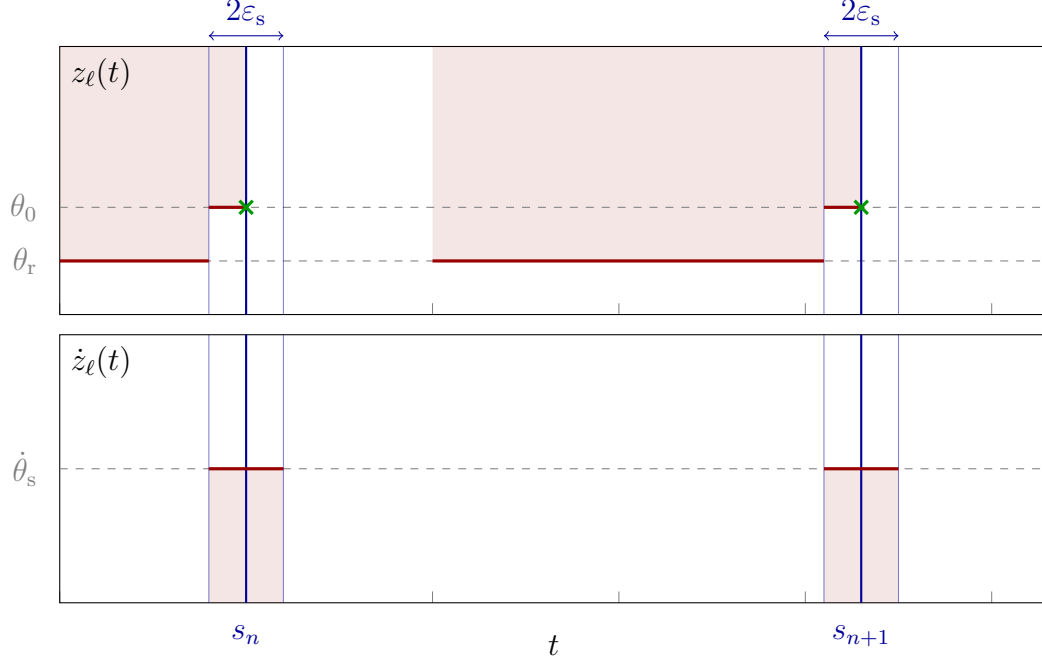


Figure 7: Conditions (8)–(10) (top) and condition (11) (bottom) for two consecutive firing times s_n and s_{n+1} . The forbidden regions are shaded in red. The point of firing is marked by a cross. The distance between the tickmarks is τ_0 .

For the numerical computations, the continuous time t in (8)–(11) is discretized with sufficient temporal resolution. Feasible weights (if they exist) can then be computed by standard software.

From the experiments in Tables 3 and 4, and from many other experiments, we observe that satisfying (8)–(12) (with sufficiently large $\dot{\theta}_s$ and sufficiently small w_b and θ_r , for all neurons simultaneously) suffices to guarantee temporal stability at some level of threshold noise. The feasibility of (8)–(12) can therefore be used as a proxy for stable memorization.

5 Memory Capacity

Clearly, for any fixed network, there must be an upper limit on the maximal period T of the memorizable content. Some pertinent (and typical) experimental results are reported in Fig. 8. In these experiments, the feasibility of (8)–(12) is used as a proxy for stable memorization (as explained above). Fig. 8 shows the probability of this feasibility as a function of T for different values of K , with other parameters as in Table 2. With Poisson parameter $\lambda = 0.2/\tau_0$, every neuron fires about 15 times per 100 τ_0 (cf. Fig. 11).

From many more such experiments (not shown here), we conclude that K is indeed the primary pertinent parameter. Both L (= the number of neurons) and d_{\max} (= the maximal axonal delay) just need to be sufficiently large (and can be traded against each other).

Note that Fig. 8 suggests that the maximal length T of stably memorizable content grows at least linearly with K . (A similar scaling was mathematically proved in a

Table 3: Effect of the minimum-slope condition (11). Every row summarizes 100 repetitions of the same experiment.

$\dot{\theta}_s \tau_0 / \theta_0$	σ_θ / θ_0	pr(20T)			rc(20T)		
		min	med	max	min	med	max
0	0.05	0.000	0.000	0.094	0.000	0.000	0.072
	0.1	0.000	0.000	0.088	0.000	0.000	0.065
	0.15	0.000	0.000	0.000	0.000	0.000	0.000
1	0.05	0.972	0.974	0.976	0.972	0.974	0.976
	0.1	0.000	0.944	0.951	0.000	0.944	0.950
	0.15	0.000	0.000	0.090	0.000	0.000	0.064
2	0.05	0.975	0.977	0.978	0.975	0.977	0.978
	0.1	0.949	0.953	0.956	0.949	0.953	0.956
	0.15	0.083	0.926	0.935	0.069	0.926	0.935

Table 4: Effect of the additional regularization by (13). Every row summarizes 100 repetitions of the same experiment.

w_b / θ_0	ν	σ_θ / θ_0	pr(20T)			rc(20T)		
			min	med	max	min	med	max
0.2	–	0.05	0.967	0.970	0.973	0.967	0.970	0.973
		0.1	0.018	0.091	0.950	0.048	0.157	0.950
		0.15	0.021	0.079	0.105	0.044	0.120	0.264
	1	0.05	0.975	0.976	0.978	0.975	0.976	0.978
		0.1	0.949	0.952	0.956	0.949	0.952	0.956
		0.15	0.071	0.923	0.931	0.093	0.922	0.931
	2	0.05	0.975	0.977	0.978	0.975	0.977	0.978
		0.1	0.949	0.953	0.956	0.949	0.953	0.956
		0.15	0.083	0.926	0.935	0.069	0.926	0.935
0.5	–	0.05	0.017	0.070	0.102	0.053	0.132	0.244
		0.1	0.014	0.066	0.100	0.056	0.136	0.258
		0.15	0.018	0.068	0.097	0.056	0.138	0.252
	1	0.05	0.972	0.974	0.976	0.972	0.974	0.976
		0.1	0.081	0.948	0.952	0.151	0.948	0.952
		0.15	0.075	0.084	0.095	0.144	0.179	0.238
	2	0.05	0.975	0.977	0.978	0.975	0.977	0.978
		0.1	0.951	0.953	0.956	0.951	0.953	0.956
		0.15	0.000	0.926	0.934	0.000	0.926	0.934

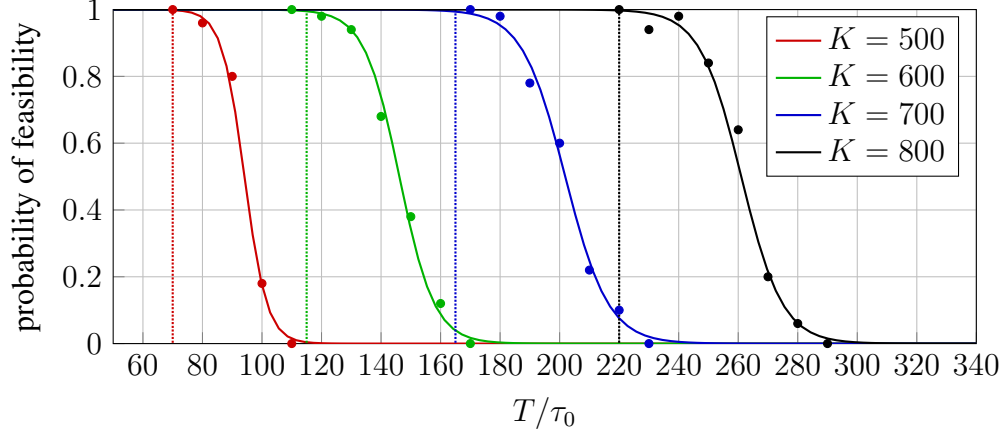


Figure 8: Empirical probability of feasibility vs. the period T , over 100 repetitions (each with a new random network and a new prescribed random spike train). The dotted vertical lines indicate the limit T_{\max} of almost sure feasibility: for $T \leq T_{\max}$, no unfeasible spike train was observed. For $T > T_{\max}$, the solid line is a logistic regression to the data points.

discrete-time setting by Murer and Loeliger (2020).)

6 Small-Jitter Analysis

A necessary condition for temporal stability is that the propagation of spike jitter through the network is damped rather than increased. For small jitter, this can be analyzed by the eigenvalues of a linearized model, as was done in (Banerjee et al., 2008). We are now going to do this as well, and we will find that satisfaction of (8)–(12) (with sufficiently large $\hat{\theta}_s$ and sufficiently small w_b and θ_r) guarantees the suppression of sufficiently small jitter, in agreement with the pertinent remarks in Sec. 4.

6.1 The Math

Let $\check{s}_0, \check{s}_1, \dots$ with $\check{s}_0 \leq \check{s}_1 \leq \dots$ be the nominal spike positions of all spikes, (i.e., the prescribed firing times of all neurons together) and let $s_n \triangleq \check{s}_n + \Delta_n$, $n = 0, 1, \dots$ be the actual spike positions. Assume that the prescribed firing score is periodic and let N be the total number of spikes in the first period. Assume that there is no threshold noise and $|\Delta_n| \ll \tau_0$ for all $n \in \{0, 1, \dots, N-1\}$. For $n \geq N$, the timing errors Δ_n , as long as their magnitude is small, propagate according to

$$\Delta_n \approx \sum_{n'=1}^N a_{n,n'} \Delta_{n-n'} \quad (14)$$

with

$$a_{n,n'} \triangleq \frac{\partial s_n}{\partial s_{n-n'}} \quad (15)$$

where we assume (without loss of essential generality) that the influence of $\Delta_{n-n'}$ for $n' > N$ can be neglected. The derivatives (15) are given by (A.9) in Appendix 7.2.

For $n \geq N$, the jitter vector $\Delta_n \triangleq (\Delta_n, \dots, \Delta_{n-N+1})^\top$ thus (approximately) evolves according to the linear recurrence

$$\Delta_n = \mathbf{A}_n \Delta_{n-1} \quad (16)$$

with

$$\mathbf{A}_n \triangleq \begin{pmatrix} a_{n,1} & \cdots & a_{n,N-1} & a_{n,N} \\ & \mathbf{I} & & \mathbf{0} \end{pmatrix} \in \mathbb{R}^{N \times N}, \quad (17)$$

where \mathbf{I} is a $(N-1) \times (N-1)$ identity matrix and $\mathbf{0}$ is an all-zeros column vector of size $N-1$. By recursion, (16) yields

$$\Delta_n = \Phi_n \Delta_N \quad (18)$$

with $\Phi_n \triangleq \mathbf{A}_n \mathbf{A}_{n-1} \cdots \mathbf{A}_{N+1}$ (for $n > N$). Since the sequence $\mathbf{A}_n, \mathbf{A}_{n+1}, \dots$ of matrices is periodic with period N , (18) can be written as

$$\Delta_n = \Phi_r \Phi_N^{q-1} \Delta_N, \quad (19)$$

where q and r are the quotient and the remainder, respectively, of the division of n by N , and $\Phi_r \triangleq \Phi_{r+N}$ for $r \leq N$.

The behavior of Δ_n for $n \rightarrow \infty$ is thus governed by the largest eigenvalue of Φ_N . Note that $(1, 1, \dots, 1)^\top$ is always an eigenvector of Φ_N with eigenvalue one (corresponding to a uniform shift of all spikes). If the magnitude of all other eigenvalues is smaller than one, then all other eigenvectors will die out, which means that the spiking score is temporally stable. Denoting the ordered (in modulus) eigenvalues of Φ_N by $\varphi_1 \geq \varphi_2 \geq \dots$, we therefore require

$$|\varphi_1| = 1 \quad \text{and} \quad |\varphi_2| < 1. \quad (20)$$

6.2 The Use

The eigenvalue condition (20) is necessary, but not sufficient, for temporal stability (with finite threshold noise variance) in the sense of Sec. 3. However, computing the eigenvalues of Φ_N is less time-consuming than, and provides complementary insight to, simulations as in Sections 3–5.

Complementing the observations in Sec. 4, we experimentally find that satisfying (8)–(12) suffices to satisfy also the eigenvalue condition (20). With the same parameters as for Tables 3 and 4, we evaluate the eigenvalues of Φ_N and report the two largest (in magnitude) $|\varphi_1|$ and $|\varphi_2|$ in Tables 5 and 6. Every row summarizes 100 repetitions of the same experiment, each with a new random network and a new random prescribed firing score; every row reports the median, the minimum, and the maximum (in magnitude) of these eigenvalues.

Note that the first row of Table 5 demonstrates that dropping the minimal-slope condition (11) makes the network unstable.

Table 5: Effect of the minimum-slope condition (11) on the eigenvalue condition (20), cf. Table 3. Every row summarizes 100 repetitions of the same experiment.

$\dot{\theta}_s \tau_0 / \theta_0$	$\log_{10} \varphi_1 $			$\log_{10} \varphi_2 $		
	min	med	max	min	med	max
0	0.5	5.3	12.0	0.0	2.3	6.1
1	0.0	0.0	0.0	-3.7	-3.5	-3.3
2	0.0	0.0	0.0	-4.0	-3.8	-3.6

Table 6: Effect of the additional regularization by (13) on the eigenvalue condition (20), cf. Table 4. Every row summarizes 100 repetitions of the same experiment.

w_b / θ_0	ν	$\log_{10} \varphi_1 $			$\log_{10} \varphi_2 $		
		min	med	max	min	med	max
0.2	–	0.0	0.0	0.0	-1.7	-1.5	-1.2
	1	0.0	0.0	0.0	-3.5	-3.3	-3.2
	2	0.0	0.0	0.0	-4.0	-3.8	-3.6
0.5	–	1.4	2.8	5.7	1.4	2.4	4.1
	1	0.0	0.0	0.0	-2.5	-2.4	-2.2
	2	0.0	0.0	0.0	-3.9	-3.8	-3.5

7 Associative Recall

As expected, memorized spike scores can be recalled by noisy partial prompts. Some pertinent experiments are described below. In these experiments, a fraction α of the neurons does not (or not always) operate in its normal mode: these αL neurons are forced to ignore their input and to produce a noisy version of their (prescribed and) memorized spike train instead. These noisy excitations are created by shifting each spike of the prescribed spike train by random zero-mean Gaussian jitter with variance σ_s^2 while preserving the refractory period τ_0 between spikes, as detailed in Appendix B.3.

7.1 Recall from Quiet State

In this experiment, the network is prepared as described in Section 4, with parameters as in Table 2. The network is started in a state of rest (with no firings and all neuron potentials set to zero), but with a fraction α of neurons forced to provide a noisy version of the memorized content as described above.

After about five periods, the precision (4) and the recall (5) have reached a steady state. In Table 7, the precision and the recall are reported, not only for the whole network but also for the αL forced neurons and the remaining autonomous neurons separately (by adapting the range of the outer sums in (4), (5), and (7) accordingly). For every set of parameters, the experiment is repeated 100 times, each with a new random network and a new random prescribed firing score; the table reports the median, the minimum, and the maximum steady-state precision and recall of all 100 repetitions.

Table 7: Recall from quiet state with $\alpha = 50\%$ forced neurons, which are forced to produce the memorized firings with jitter parameter $\sigma_s/\tau_0 = 0.1$. Each group of three rows summarizes 100 repetitions of the same experiment.

σ_θ/θ_0	group	pr($10T$)			rc($10T$)		
		min	med	max	min	med	max
0.05	forced	0.824	0.843	0.855	0.824	0.843	0.855
	autonomous	0.956	0.961	0.966	0.956	0.961	0.966
	all	0.890	0.901	0.907	0.890	0.901	0.907
0.10	forced	0.824	0.843	0.855	0.824	0.843	0.855
	autonomous	0.939	0.944	0.948	0.939	0.944	0.948
	all	0.883	0.892	0.899	0.883	0.892	0.899
0.20	forced	0.824	0.843	0.855	0.824	0.843	0.855
	autonomous	0.667	0.816	0.908	0.319	0.710	0.907
	all	0.750	0.822	0.873	0.573	0.770	0.871

Note that the temporal accuracy of the autonomously operating neurons exceeds the temporal accuracy of the excitation.

7.2 Switching Between Memorized Content

In this experiment, the memorized random score of firings consists of two segments \check{x}_R and \check{x}_B , each of which is periodic with period $T = 50 \tau_0$. A fraction α of neurons (henceforth called the forceable neurons) is sometimes forced to produce noisy memorized contents as in Section 7.1.

The network is started in a state of rest, with no firings and all neuron potentials set to zero. The simulation proceeds in different phases of duration T . In each such phase, the network operates in one of the following three modes:

- (1) Autonomously as in Sec. 2.
- (2) The forceable neurons are forced to produce a noisy version of \check{x}_R .
- (3) The forceable neurons are forced to produce a noisy version of \check{x}_B .

Numerical results of such an experiment with $\alpha = 0.75$ are shown in Fig. 9.

Conclusion

We have demonstrated (with numerical experiments) that continuous-time neural networks with random (but fixed) transmission delays can store and autonomously reproduce any given random spike trains up to some maximal length T_{\max} , with stable accurate relative timing of all spikes, with probability close to one. Moreover, these experiments suggest that T_{\max} scales at least linearly with the number of synaptic inputs per neuron.

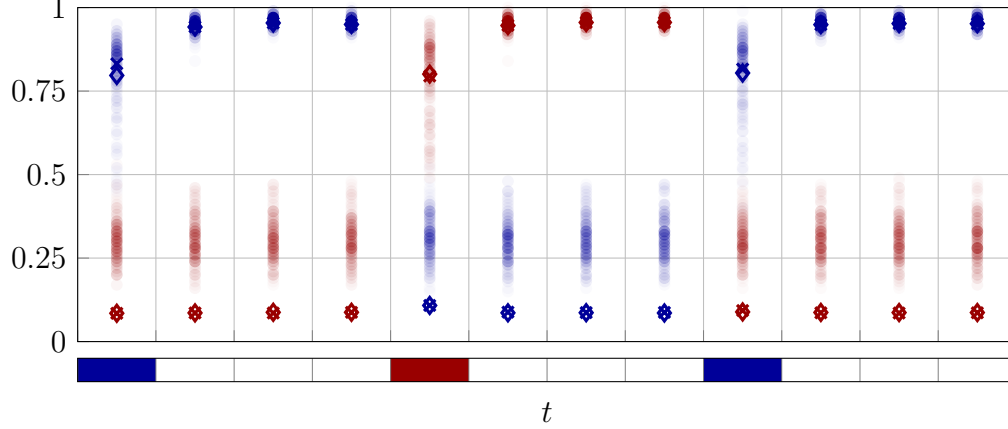


Figure 9: Switching between memorized firing scores \check{x}_B (blue) and \check{x}_R (red), with $\alpha = 75\%$ forceable neurons and with jitter parameter $\sigma_s/\tau_0 = 0.1$. The bar at the bottom shows when and how the network is prompted. Precision (crosses) and recall (diamonds) with respect to \check{x}_B and \check{x}_R are shown for each period. In addition, either per-neuron recall or per-neuron precision (whichever is smaller) are displayed using transparent circles, with opacity indicating neuron density. The distance between the tickmarks is T .

In these experiments, the required synaptic weights are computed offline⁴, to satisfy a template that encourages temporal stability.

In summary, our experiments demonstrate that clockless continuous-time networks can operate with spike-level temporal stability almost like digital processors. We do not know if this possibility is used in biological neural networks, but it does seem to open interesting perspectives for neuromorphic engineering.

Appendix A: The Derivatives (15)

Recall the setting of (15), with nominal spike times $\check{s}_0, \check{s}_1, \dots$ (with $\check{s}_0 \leq \check{s}_1 \leq \dots$), actual spike times $s_0 = \check{s}_0 + \Delta_0, s_1 = \check{s}_1 + \Delta_1, \dots$, and no threshold noise. Let N be the number of spikes in the first period.

Let $z_{\ell(n)}(t)$ be the potential of the neuron that produces the firing at time s_n . For $n > N$, we can write

$$z_{\ell(n)}(t) = \sum_{n'=1}^N z_{n,n'}(t), \quad (\text{A.1})$$

where $z_{n,n'}(t)$ is the contribution to $z_{\ell(n)}(t)$ by the spike at time $s_{n-n'}$. Let $\check{z}_{\ell(n)}(t)$ and $\check{z}_{n,n'}(t)$ be the nominal values of $z_{\ell(n)}(t)$ and $z_{n,n'}(t)$, respectively. Since there is no threshold noise, we have both $z_{\ell(n)}(s_n) = \theta_0$ and $\check{z}_{\ell(n)}(\check{s}_n) = \theta_0$ for all n . Note also that

$$z_{n,n'}(t) = \check{z}_{n,n'}(t - \Delta_{n-n'}). \quad (\text{A.2})$$

In the following, $\dot{\check{z}}_{n,n'}(t)$ denotes the derivative of $\check{z}_{n,n'}(t)$. Linearizing (A.1) around the nominal firing time $\check{s}_{\ell(n)}$ yields

⁴The computation of the weights can be reformulated as a neuron-local online algorithm, but this possibility was not elaborated in this paper.

$$z_{\ell(n)}(\check{s}_n + \Delta_n) = \sum_{n'} z_{n,n'}(\check{s}_n + \Delta_n) \quad (\text{A.3})$$

$$= \sum_{n'} \check{z}_{n,n'}(\check{s}_n + \Delta_n - \Delta_{n-n'}) \quad (\text{A.4})$$

$$\approx \sum_{n'} \check{z}_{n,n'}(\check{s}_n) + \sum_{n'} (\Delta_n - \Delta_{n-n'}) \dot{\check{z}}_{n,n'}(\check{s}_n) \quad (\text{A.5})$$

$$= \check{z}_{\ell(n)}(\check{s}_n) + \sum_{n'} (\Delta_n - \Delta_{n-n'}) \dot{\check{z}}_{n,n'}(\check{s}_n) \quad (\text{A.6})$$

$$= \theta_0 + \sum_{n'} (\Delta_n - \Delta_{n-n'}) \dot{\check{z}}_{n,n'}(\check{s}_n). \quad (\text{A.7})$$

Solving $z_{\ell(n)}(\check{s}_n + \Delta_n) = \theta_0$ for Δ_n then yields

$$\Delta_n = \sum_{n'=1}^N a_{n,n'} \Delta_{n-n'} \quad (\text{A.8})$$

with

$$a_{n,n'} = \frac{\dot{\check{z}}_{n,n'}(s_n)}{\sum_{n'} \dot{\check{z}}_{n,n'}(s_n)} \quad (\text{A.9})$$

Finally, from (2), we have

$$\dot{\check{z}}_{n,n'}(s_n) = \sum_{k \in \mathcal{K}(n,n')} w_{\ell(n),k} \dot{h}(s_n - d_{\ell(n),k} - s_{n-n'}), \quad (\text{A.10})$$

where $\mathcal{K}(n, n')$ is the set of indices k such that the firing at time $s_{n-n'}$ contributes to $z_{\ell(n)}(t)$ via $\tilde{x}_{\ell(n),k}$.

Appendix B: The Random Periodic Spike Trains

In this section, we provide the definition of, and the sampling algorithm for, the periodic random spike trains that are used in this paper as described in Section 3.2.

As stated in Section 3.2, the random spike trains for the different neurons are statistically independent. Therefore, it suffices to consider here only a single spike train (i.e., a single neuron).

The basic idea is to modify the definition of stationary Poisson process with firing rate λ such that

- it is periodic (with period T), and
- it respects the refractory period, i.e., any two spikes are separated by at least τ_0 .

The pertinent math is given in Sections B.1 and B.2. The resulting sampling algorithm is given in Section B.3. The expected number of spikes per period is given by (B.13) below.

B.1 Poisson Process Basics

In a (standard stationary) Poisson process with firing rate $\lambda > 0$, the number of firings N in an interval of duration T is a random variable, and the probability of exactly n firings is

$$P(N = n) = \gamma_P \frac{(\lambda T)^n}{n!} \quad (\text{B.1})$$

with scale factor $\gamma_P = \exp(-\lambda T)$. In order to suitably modify (B.1) for our purpose, we need to dig a little deeper. Divide T into K subintervals of length T/K and let N_K be the (random) number of firings in some fixed subinterval. For large K , each subinterval contains at most one firing, i.e.,

$$P(N_K > 1) \ll P(N_K = 1) \approx \lambda T/K \quad (\text{B.2})$$

(which becomes exact in the limit $K \rightarrow \infty$), and (B.1) can be recovered from (B.2) by

$$P(N = n) = \lim_{K \rightarrow \infty} \binom{K}{n} \left(\frac{\lambda T}{K} \right)^n \left(1 - \frac{\lambda T}{K} \right)^{K-n}. \quad (\text{B.3})$$

B.2 The Modification

We keep the probability measure of the Poisson process over $[0, T)$ except that we forbid all configurations that violate the refractory period. Specifically, we replace (B.3) by

$$P(N = n) = \tilde{\gamma} \lim_{K \rightarrow \infty} C(K, n) \left(\frac{\lambda T}{K} \right)^n \left(1 - \frac{\lambda T}{K} \right)^{K-n}, \quad (\text{B.4})$$

where $C(K, n)$ is the number of configurations (with at most one firing per subinterval and n firings in total) with at least $K\tau_0/T$ empty subintervals between firings. The scale factor $\tilde{\gamma}$ is required for (B.4) to be properly normalized.

In order to determine $C(K, n)$, we note that there is a one-to-one correspondence (illustrated in Fig. 10) between

- (a) configurations of n spikes on the interval $[0, T)$ such that (i) there is a spike at 0 and (ii) each spike is followed by a refractory period of length τ_0 , and
- (b) configurations of n spikes on the interval $[0, T - n\tau_0)$ with a spike at 0.

Counting the latter is obvious: there are

$$(K_n - 1)(K_n - 2) \cdots (K_n - n + 1) \quad (\text{B.5})$$

such ordered configurations where

$$K_n \triangleq \left\lfloor K \left(1 - \frac{n\tau_0}{T} \right) \right\rfloor. \quad (\text{B.6})$$

Dropping the constraint that the first spike occurs at time 0 and passing to unordered configurations yields

$$C(K, n) = \frac{K(K_n - 1)(K_n - 2) \cdots (K_n - n + 1)}{n!} \quad (\text{B.7})$$

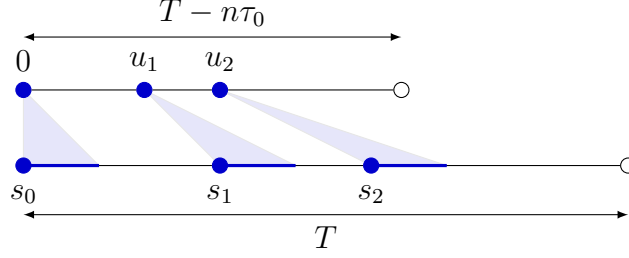


Figure 10: The one-to-one correspondence of configurations in Appendix B.2.

with $C(K, 0) = 1$. For $n > 0$, we have

$$P(N = n) = \tilde{\gamma} \lim_{K \rightarrow \infty} C(K, n) \left(\frac{\lambda T/K}{1 - \lambda T/K} \right)^n \left(1 - \frac{\lambda T}{K} \right)^K, \quad (\text{B.8})$$

$$= \tilde{\gamma} \lim_{K \rightarrow \infty} C(K, n) \left(\frac{\lambda T}{K} \right)^n e^{-\lambda T} \quad (\text{B.9})$$

$$= \tilde{\gamma} \frac{\left(1 - \frac{n\tau_0}{T}\right)^{n-1}}{n!} (\lambda T)^n e^{-\lambda T} \quad (\text{B.10})$$

$$= \tilde{\gamma} \frac{(\lambda(T - n\tau_0))^{n-1}}{n!} \lambda T e^{-\lambda T}, \quad (\text{B.11})$$

which happens to hold also for $n = 0$. We thus have

$$P(N = n) = \begin{cases} \gamma \frac{(\lambda(T - n\tau_0))^{n-1}}{n!}, & \text{if } 0 \leq n < T/\tau_0 \\ 0, & \text{if } n \geq T/\tau_0, \end{cases} \quad (\text{B.12})$$

where the scale factor γ is determined by $\sum_n P(N = n) = 1$. Note that $P(N=0) = \gamma(\lambda T)^{-1}$. Note also that (B.12) agrees with (B.1) for $\tau_0 = 0$ and $\gamma = \gamma_p \lambda T$.

The expected number of spikes per period is

$$\mathbb{E}(N) = \sum_n n P(N = n). \quad (\text{B.13})$$

Numerical examples of (B.12) and (B.13) are given in Fig. 11.

B.3 The Sampling Algorithm

We thus arrive at the following sampling algorithm.

1. Sample the number of spikes n per period according to (B.12). If $n = 0$, return an empty spike train.
2. Sample s_0 , the position of the first spike, uniformly on $[0, T)$.
3. Sample u_1, u_2, \dots, u_{n-1} independently and uniformly on $[0, T - n\tau_0]$, and (with a slight abuse of notation) sort them such that $u_1 < u_2 < \dots < u_{n-1}$.
4. For $n' = 1, \dots, n-1$, the firing times are $s_{n'} = s_0 + n'\tau_0 + u_{n'}$ (cf. Fig. 10).
5. Periodically extend s_0, s_1, \dots, s_{n-1} .

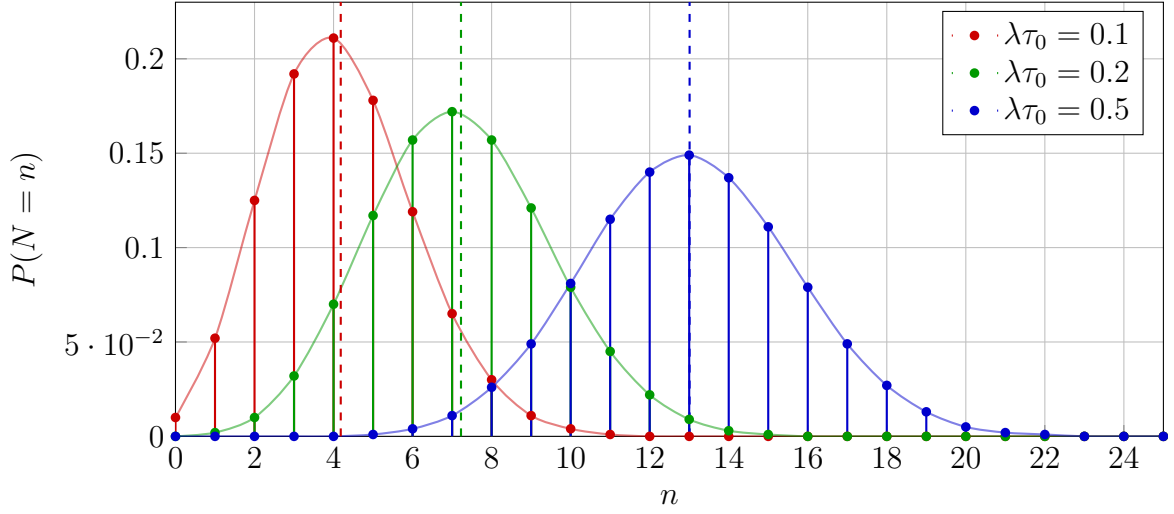


Figure 11: The probability mass function (B.12) with $T = 50 \tau_0$ for different values of $\lambda \tau_0$. The expected number of spikes (B.13) is shown as a vertical dashed line.

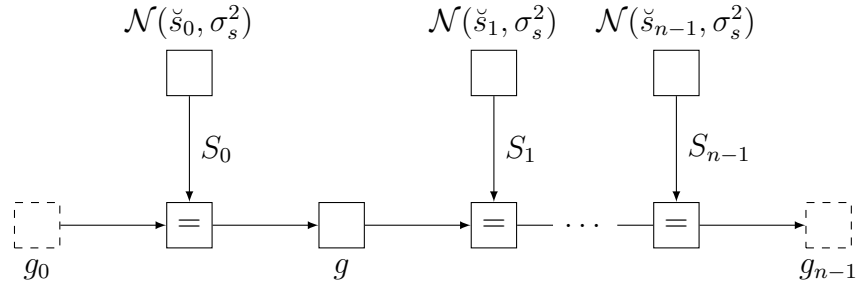


Figure 12: Factor graph (Loeliger, 2004) of the joint probability density function of S_0, \dots, S_{n-1} with $g \triangleq \mathbb{1}[S_{n'} - S_{n'-1} > \tau_0]$ for $n' = 1, \dots, n-1$, and optional additional constraints on S_0 and S_{n-1} expressed by g_0 and g_{n-1} , respectively.

Appendix C: Adding Spike Jitter Respecting the Refractory Period

For the experiments in Section 7, the noisy spike times s_0, \dots, s_{n-1} are obtained from the nominal spike times $\check{s}_0, \dots, \check{s}_{n-1}$ by adding zero-mean Gaussian jitter with variance σ_s^2 while maintaining the constraint that s_0, \dots, s_{n-1} are separated by at least τ_0 . A factor graph of the pertinent joint probability density function is shown in Fig. 12.

Sampling from this distribution can be done by Gibbs sampling (Geman & Geman, 1984) as follows.⁵ For $m = 1, 2, \dots, M \gg 1$, alternate the following two steps, beginning with $s_k^{(0)} = \check{s}_k$ for all k :

1. For even indices k , sample $s_k^{(m)}$ from a Gaussian with mean \check{s}_k and variance σ_s^2 ,

⁵The extension to constrained first and/or last spike, e.g., minimum starting time or periodicity requirement, is straightforward.

truncated to the interval $(s_{k-1}^{(m-1)} + \tau_0, s_{k+1}^{(m-1)} - \tau_0)$.

2. For odd indices k , sample $s_k^{(m)}$ from a Gaussian with mean \check{s}_k and variance σ_s^2 , truncated to the interval $(s_{k-1}^{(m)} + \tau_0, s_{k+1}^{(m)} - \tau_0)$.

Return $s_k = s_k^{(M)}$ for all k .

As always with Gibbs sampling, it is difficult to know how large M needs to be. The experiments in Section 7 were done with $M = 1000$.

Acknowledgment

The paper builds on the foundations laid by Patrick Murer (Murer, 2022), who also helped to get the present work started. We also wish to thank Hampus Malmberg for guidance and support.

References

- Amit, D. J. (1989). *Modeling Brain Function: The World of Attractor Neural Networks*, Cambridge University Press.
- Banerjee, A., Seriès, P., & Pouget, A. (2008). Dynamical constraints on using precise spike timing to compute in recurrent cortical networks. *Neural Computation*, 20 (4), 974–993.
- Dalgaty, T., et al. (2024). Mosaic: in-memory computing and routing for small-world spike-based neuromorphic systems. *Nature Communications*, 15 (142), 1–12.
- Eliasmith, C. (2005). A unified approach to building and controlling spiking attractor networks. *Neural Computation*, 17 (6), 1276–1314.
- Faisal, A. A., Selen, L. P. J., & Wolpert, D. M. (2008). Noise in the nervous system. *Nature Reviews Neuroscience*, 9, 292–303.
- Geman, S. & Geman, D. (1984). Stochastic relaxation, Gibbs distributions, and the Bayesian restoration of images. *IEEE Transactions on Pattern Analysis and Machine Intelligence*, 6 (6), 721–741.
- Gerstner, W. (1995). Time structure of the activity in neural network models. *Physical Review E*, 51 (1), 738–758.
- Grimaldi, A. et al. (2023). Precise spiking motifs in neurobiological and neuromorphic data. *Brain Science*, 13 (68)
- Hopfield, J. J. (1982). Neural networks and physical systems with emergent collective computational abilities. *Proceedings of the National Academy of Sciences*, 79 (8), 2554–2558.

- Indiveri, G. & Liu, S.-C. (2015). Memory and information processing in neuromorphic systems. *Proceedings of the IEEE*, 103 (8), 1379 – 1397.
- Izhikevich, E. M. (2006). Polychronization: Computation with spikes. *Neural Computation*, 18 (2), 245–282.
- Kandel, E. R., Koester, J. D., Mack, S. H., & Siegelbaum, S. A. (2021). *Principle of Neural Science*, 6th ed., McGraw-Hill.
- Kistler, W. M., Gerstner, W., & van Hemmen, J. L. (1997). Reduction of the Hodgkin-Huxley equations to a single-variable threshold model. *Neural Computation*, 9 (5), 1015–1045.
- Lee, W. W., Kukreja, S. L., & Thakor, N. V. (2017). CONE: Convex optimized-synaptic efficacies for temporally precise spike mapping. *IEEE Transactions on Neural Networks and Learning Systems*, 28 (4), 849–861.
- Loeliger, H.-A. (2004). An introduction to factor graphs. *IEEE Signal Processing Magazine*, 21 (1), 28–41.
- Murer, P. (2022). *A New Perspective on Memorization in Recurrent Networks of Spiking Neurons*. Ph.D. Thesis, no. 28166, ETH Zurich.
- Murer, P. & Loeliger, H.-A. (2020). Online memorization of random firing sequences by a recurrent neural network, *2020 IEEE International Symposium on Information Theory (ISIT)*, June 21-26, 2020.
- Poucet, B. & Save, E. (2005). Attractors in memory. *Science*, 308 (5723), 799 – 800.
- Ramsauer, H., et al. (2021). Hopfield networks is all you need. *arXiv*.
- Rubino, A., Cartiglia, M., Payvand, M., & Indiveri, G. (2023). Neuromorphic analog circuits for robust on-chip always-on learning in spiking neural networks. *2023 IEEE 5th International Conference on Artificial Intelligence Circuits and Systems (AICAS)*, Hangzhou, China, 1–5.
- Wang, X., Lin, X., & Dang, X. (2020). Supervised learning in spiking neural networks: A review of algorithms and evaluations. *Neural Networks*, 125, 258–280.